AFRL-RX-WP-TM-2014-0085

TEMPORAL EVOLUTION OF NON-EQUILIBRIUM γ' PRECIPITATES IN A RAPIDLY QUENCHED NICKEL BASE SUPERALLOY (PREPRINT)

J. Tiley
AFRL/RXCM

T. Rojhirunsakool, A.R.P. Singh, S. Nag and R. Banerjee
University of North Texas

J.Y. Hwang
Korean Institute of Science and Technology

APRIL 2014
Final Report

Approved for public release; distribution unlimited.

See additional restrictions described on inside pages

STINFO COPY

AIR FORCE RESEARCH LABORATORY
MATERIALS AND MANUFACTURING DIRECTORATE
WRIGHT-PATTERSON AIR FORCE BASE, OH 45433-7750
AIR FORCE MATERIEL COMMAND
UNITED STATES AIR FORCE

NOTICE AND SIGNATURE PAGE

AFRL-RX-WP-TM-2014-0085 HAS BEEN REVIEWED AND IS APPROVED FOR PUBLICATION IN ACCORDANCE WITH ASSIGNED DISTRIBUTION STATEMENT.

//Signature//

JAIMIE TILEY, Project Engineer
Metals Branch
Structural Materials Division

//Signature//

DANIEL EVANS, Chief
Metals Branch
Structural Materials Division

//Signature//

ROBERT T. MARSHALL, Deputy Chief
Structural Materials Division
Materials and Manufacturing Directorate

REPORT DOCUMENTATION PAGE

Form Approved
OMB No. 0704-0188

1. REPORT DATE *(DD-MM-YY)*	2. REPORT TYPE	3. DATES COVERED *(From - To)*
April 2014	Final	01 December 2009 – 31 March 2014

4. TITLE AND SUBTITLE
TEMPORAL EVOLUTION OF NON-EQUILIBRIUM γ' PRECIPITATES IN A RAPIDLY QUENCHED NICKEL BASE SUPERALLOY (PREPRINT)

5a. CONTRACT NUMBER In-house
5b. GRANT NUMBER
5c. PROGRAM ELEMENT NUMBER 62102F

6. AUTHOR(S)
J. Tiley - AFRL/RXCM
T. Rojhirunsakool, A.R.P. Singh, S. Nag and R. Banerjee -University of North Texas
J.Y. Hwang - Korean Institute of Science and Technology

5d. PROJECT NUMBER 4347
5e. TASK NUMBER
5f. WORK UNIT NUMBER X0DE

7. PERFORMING ORGANIZATION NAME(S) AND ADDRESS(ES)
AFRL/RXCM
2941 Hobson Way
Wright-Patterson AFB OH 45433-7750

See back

8. PERFORMING ORGANIZATION REPORT NUMBER

9. SPONSORING/MONITORING AGENCY NAME(S) AND ADDRESS(ES)
Air Force Research Laboratory
Materials and Manufacturing Directorate
Wright-Patterson Air Force Base, OH 45433-7750
Air Force Materiel Command
United States Air Force

10. SPONSORING/MONITORING AGENCY ACRONYM(S) AFRL/RXCM

11. SPONSORING/MONITORING AGENCY REPORT NUMBER(S) AFRL-RX-WP-TM-2014-0085

12. DISTRIBUTION/AVAILABILITY STATEMENT
Approved for public release; distribution unlimited.

13. SUPPLEMENTARY NOTES
PA Case Number: 88ABW-2013-3936; Clearance Date: 04 September 2013. Journal article to be published in *Journal of Alloys and Compounds*. This is a work of the U.S. Government and is not subject to copyright protection in the United States. Document contains color.

14. ABSTRACT (*Maximum 200 words*)
The temporal evolution of non-equilibrium γ' precipitates in a rapidly quenched and isothermally annealed commercial nickel base superalloy has been investigated by coupling transmission electron microscopy and atom probe tomography. When subjected to rapid quenching from above the γ' solvus temperature, the supersaturated single phase γ matrix appears to undergo compositional phase separation possibly via spinodal decomposition to form solute-rich and solute-depleted regions. The regions that have an excess of Al and Ti (depleted in Cr and Co) undergo an ordering process resulting in the γ' domains which exhibit a far-from equilibrium composition. Furthermore, only local equilibrium is observed near the γ/γ' interface, with the far-field γ composition being far from equilibrium at the early stages of annealing. Upon isothermal annealing, the γ/γ' interface sharpens and the compositions of both γ and γ' phases approach equilibrium. The influence of a non-classical mechanism of γ' precipitation on the size distribution of precipitates as well as the precipitate and matrix compositions, and its subsequent evolution during isothermal annealing has been discussed.

15. SUBJECT TERMS
gamma prime evolution, nickel base superalloys, atom probe tomography

16. SECURITY CLASSIFICATION OF:			17. LIMITATION OF ABSTRACT:	18. NUMBER OF PAGES	19a. NAME OF RESPONSIBLE PERSON (Monitor)
					Jaimie Tiley
a. REPORT	b. ABSTRACT	c. THIS PAGE	SAR	21	19b. TELEPHONE NUMBER *(Include Area Code)*
Unclassified	Unclassified	Unclassified			(937) 255-7416

REPORT DOCUMENTATION PAGE Cont'd

6. AUTHOR(S)

7. PERFORMING ORGANIZATION NAME(S) AND ADDRESS(ES)

University of North Texas
Center for Advanced Research and Technology and
Department of Materials Science and Engineering
1155 Union Circle
Denton, TX 76203-5017

Korea Institute of Science and Technology
Carbon Convergence Materials Research Center
Korea

Temporal evolution of non-equilibrium γ' precipitates in a rapidly quenched nickel base superalloy

T. Rojhirunsakool, A.R.P. Singh, S. Nag, J.Y. Hwang[a], J. Tiley[b], R. Banerjee
Center for Advanced Research and Technology and Department of Materials Science and Engineering
University of North Texas, Denton TX, U.S.A.
[a] Carbon Convergence Materials Research Center, Korean Institute of Science and Technology, Korea
[b] Air Force Research Laboratory, Dayton, OH, U.S.A.

Abstract

The temporal evolution of non-equilibrium γ' precipitates in a rapidly quenched and isothermally annealed commercial nickel base superalloy has been investigated by coupling transmission electron microscopy and atom probe tomography. When subjected to rapid quenching from above the γ' solvus temperature, the supersaturated single phase γ matrix appears to undergo compositional phase separation possibly via spinodal decomposition to form solute-rich and solute-depleted regions. The regions that have an excess of Al and Ti (depleted in Cr and Co) undergo an ordering process resulting in the γ' domains which exhibit a far-from equilibrium composition. Furthermore, only local equilibrium is observed near the γ/γ' interface, with the far-field γ composition being far-from equilibrium at the early stages of annealing. Upon isothermal annealing, the γ/γ' interface sharpens and the compositions of both γ and γ' phases approach equilibrium. The influence of a non-classical mechanism of γ' precipitation on the size distribution of precipitates as well as the precipitate and matrix compositions, and its subsequent evolution during isothermal annealing has been discussed.

Introduction

The microstructure, in case of most nickel base superalloys, primarily consists of finely dispersed precipitates of the ordered γ' phase, having an $L1_2$ structure, within a disordered face-centered cubic (FCC) γ matrix. When a disordered solid solution is rapidly quenched from the single γ phase field to room temperature, it results in a two-phase mixture of γ and γ's. However, the highly supersaturated and undercooled single γ phase is often unstable, more precisely metastable, with respect to the ensuing ordering or phase separation [1]. The decomposition of the supersaturated γ solid solution may take place via multiple transformation pathways. In the past, significant research efforts have been devoted to investigate the precipitation mechanism of the γ' phase [1-6]. In most cases, the FCC to $L1_2$ transformation is a first order transition, involving classical nucleation and growth, wherein precipitates of the ordered γ' phase with a near-equilibrium composition will be randomly nucleated throughout the matrix. A second pathway is where the supersaturated γ solid solution undergoes spinodal decomposition to form solute-rich and solute-depleted regions, followed by ordering within typically those regions that are richer in solutes such as Al and Ti [1,7-12]. Similar study on phase separation in the Fe-Cr system has been reported where statistical analysis of concentration frequency distribution was used to detect phase separation at the early stages of coarsening [13]. Other alternative pathways include decomposition wherein the degree of ordering continuously increases [14] or decomposition that occurs via congruent ordering before phase separation [2,6,15,16].

Pareige et al. [17] have reported ordering and phase separation taking place in a model Ni-Cr-Al alloy using a combined Monte Carlo (MC) simulation and experimental approach that included results from atom probe tomography (APT). Their results indicate that the precipitation mechanism of the γ' phase occurs via classical nucleation and growth in a low supersaturated Ni-Cr-Al alloy, whereas decomposition of a high supersaturated alloy takes place via congruent ordering followed by phase separation. A more recent study, carried out by Viswanathan et al. [9], investigated the precipitation mechanism of the γ' phase in a rapidly quenched commercially used Ni-based superalloy, Rene 88 DT. The experimental observations indicate that phase separation occurring in the γ matrix develops nanometer scale domains that are depleted in Co, Cr, and Mo. The concentration of Al and Ti showed a reverse trend in these domains. The Cr depleted domains, which are also depleted in Co and Mo and enriched in Ti and Al, subsequently undergo chemical ordering to form γ' precipitates exhibiting the $L1_2$ ordered structure. The presence of such ordering was observed via high resolution scanning transmission electron microscopy (STEM), where the ordered regions were only confined within the Cr-depleted pockets. Also APT results showed that the Cr-rich and Cr-depleted domains were interconnected and exhibited compositions that were far-from-equilibrium. Coupling the two observations presented above, Viswanathan et.al. suggested the possibility of phase separation within the γ matrix preceding the ordering process in fast quenched Rene 88 DT [4].

The present study focuses on the formation and temporal evolution of ordered γ' precipitates with far-from-equilibrium compositions resulting from rapid quenching from supersolvus temperatures. This study couples transmission electron microscopy (TEM) as well as the APT technique to study the atomic-scale structural and compositional changes associated with isothermal annealing of rapidly quenched Rene 88DT.

Experimental Procedures and Methods

Experiments were carried out on a commercially procured Rene 88 DT alloy with a nominal composition of 56.53Ni-16.24Cr-13.27Co-3.92Ti-2.09Al-4.08Mo-3.92W-0.76Nb (wt%) or 55.63Ni-18.02Cr-13.00Co-4.74Ti-4.45Al-2.48Mo-1.21W-0.46Nb (at%). The sample material was cut and subsequently γ solution heat treated in the single γ phase field at 1150 °C for 60 min in vacuum and subsequently rapidly quenched in ice-water under an inert argon atmosphere. After quenching, samples were subjected to isothermal annealing at 760 °C for 1, 5, 30, or 60 min, respectively. Additionally, another sample (SC 50) was annealed for 50 hr at 760 °C. Samples for TEM were prepared via conventional methods consisting of mechanical grinding, followed by dimple grinding, and finally ion-beam milling until the sample was electron transparent. Ion-beam milling was facilitated by low energy argon on a Fischione model 1010 system. TEM sample observations were conducted on a FEI Tecnai F20 field-emission gun TEM, operated at 200 kV. Samples for APT were prepared using the dual-beam focused ion beam (FIB) technique using a FEI Nova Nanolab 200 system. The final tip diameter of the atom probe specimens was 50-70 nm. APT experiments were conducted using a CAMECA LEAP 3000X HR instrument. All APT experiments were carried out in the voltage evaporation mode at a temperature of 50 K with a pulse rate of 160 KHz and target evaporation of 0.5%. Data analyses were carried out using CAMECA IVAS 3.6 software.

Results and Discussion

Rapidly quenched condition

Fig. 1(a) shows a selected area diffraction (SAD) pattern of extreme water quenched (EWQ) Rene 88 DT sample recorded along the <001> zone axis. In this diffraction pattern, the presence of <100> and <110> superlattice spots, along with the fundamental γ reflections, indicates an $L1_2$-type ordered γ' precipitation forming during quenching from the supersolvus temperature. However, the SAD pattern shows no evidence of satellite reflections around the primary matrix reflections, which is typically the signature of phase separation via spinodal decomposition.

The compositional analyses of the rapidly quenched γ' precipitates has been carried out using APT. The γ/γ' interfaces have been delineated by selecting an appropriate Cr iso-concentration value [18]. Cr was chosen as the preferred element as it strongly partitions between the γ and γ' phases in this alloy. Fig. 1(b) shows a three dimensional reconstruction where an isosurface generated using Cr = 14 at% has been superimposed on the Ni atoms (green). The corresponding two-dimensional Cr concentration map is also shown in this figure. Both the 3D reconstruction as well as the 2D compositional map in Fig. 1(b) reveal the interconnectivity between Cr-rich and Cr-depleted pockets. This is quite similar to the HAADF-HRSTEM observation in [9] and can be related to the nano-scale composition modulation developing in the quenched alloy, a possible indicator of the early stages of spinodal decomposition. It is worth noting that the composition modulation observed in the APT results presented in this paper as well as from the HRSTEM observations discussed previously [4] are not associated to a particular elastically soft direction, namely <100> in case of cubic phases. Furthermore, the regions with less than 14 % Cr, enclosed by concave interfaces in the 3D APT reconstruction shown in Fig. 1(b) and the darker pockets in 2D composition map shown below, are very similar in size-scale to the ordered domains observed in the aberration-corrected HAADF-STEM images reported previously [4]. Thus, it can be deduced that these Cr-depleted regions correspond to the γ' precipitates while the regions having more than 14 %Cr correspond to the γ matrix. The partitioning of the primary alloying elements across the γ/γ' interface has been plotted as a proximity histogram, generated using a Cr = 14 at% isosurface (Fig. 1(c)) [18]. The proxigram clearly shows the partitioning of Cr at a nanometer scale even though a rapid cooling rate was experienced by this sample. While there is significant partitioning of the major alloying elements such as Cr, Co, and Al, the compositional gradient across the γ/γ' interface is very diffuse, and the γ' precipitates exhibit a far-from-equilibrium composition in this case. For reference, the near-equilibrium composition of γ' precipitates in Rene 88DT has been determined from precipitates slow-cooled from a supersolvus temperature and subsequently annealed at 760 °C for 50 hrs [19]. The composition of the γ' precipitates in both conditions are listed in Table 1. These APT results corroborate the previously reported decomposition pathway involving the development of a composition modulation within the γ matrix followed by the γ to γ' transformation within the Cr depleted regions [4].

Morphological changes during isothermal annealing

Figs. 2(a) and (b) show dark field TEM images recorded using one of the {100} superlattice reflections in <001> zone axis for Rene 88 DT samples that were rapidly quenched and subsequently annealed at 760 ºC for 1 min (EWQ+1) and 5 min (EWQ+5), respectively. Similarly, Figs. 2(c) and (d) show dark field TEM images obtained using {111} superlattice reflection in <011> zone axis for samples that were annealed at 760ºC for 30 min (EWQ+30) and 60 min (EWQ+60), respectively. The corresponding SAD patterns are shown as insets in Fig. 2. The γ' precipitates first appear as discrete particles after annealing for 1 min and 5 min, respectively, as shown in Figs. 2a and 2b, and substantially grow and coarsen after annealing for 30 and 60 min (Figs. 2c and 2d). It is worth noting that the dark field TEM images in Fig. 2 have been obtained using only one superlattice reflection, thus capturing the volume fraction corresponding to just one variant of γ' precipitates. Thus, the actual number density of γ' precipitates are much higher than what they appear in Fig. 2. The annealed EWQ series of samples exhibit nearly spherical morphologies. Fig. 3(a)-(d) show size distribution plots of γ' precipitates obtained from dark field TEM images for samples that were annealed at 760ºC for 1 min (EWQ+1), 5 min (EWQ+5), 30 min (EWQ+30), and 60 min (EWQ+60), respectively. The γ' precipitates show a unimodal size distribution for all of the annealing times. Average equivalent γ' precipitate diameters from isothermal annealing for 1 min, 5 min, 30 min, and 60 min are 1.94, 2.04, 3.35, and 3.56 nm, respectively. This result indicates that the precipitates size of the γ' phase increases with increasing annealing time. Furthermore, a significant change in the size of the γ' precipitates occurs between 5 and 30 min.

Compositional analysis during isothermal annealing

Fig. 4(a)-(d) show APT reconstructions using a 14at%Cr isosurface (blue) superimposed on Ni ions (green) of the samples which were isothermally annealed at 760°C for 1min (EWQ+1), 5min (EWQ+5), 30min (EWQ+30) and 60min (EWQ+60), respectively. The isosurfaces delineate multiple fine-scale γ' precipitates for all annealing times. The APT reconstructions corresponding to the EWQ+1 and EWQ+5 samples clearly show an increase in the size of γ' precipitates without being interconnected in nature as observed in case of the as quenched sample (EWQ). For all the annealing times, the corresponding proxigrams are plotted in the same figure (Fig. 4) generated from the 14 at%Cr isosurface. As observed from Figs. 4(a) and (b), during the early stages of annealing (1min and 5mins), the compositional gradient across the γ/γ' interface is very diffuse. However for longer annealing times, the γ/γ' interface width becomes sharper. Since Cr exhibits the largest partitioning across the γ/γ' interfaces, the corresponding interface widths for all annealing times have been calculated based on the Cr composition profile. The compositional width of the γ/γ' interface was determined using a method that uses 90% of the steady state γ and 10% of steady state γ' compositions[19-21]. The γ/γ' interface width changes from 2.4 in EWQ to 1.6 in EWQ+60 condition. The summary of these results has been compiled in Table 3. It is to be noted that as these interface widths were measured from the proximity histogram profiles, they have been averaged for all different vectors drawn perpendicular to the precipitate-matrix interface. Thus the overall error associated with such an approach is very minimal.

In all four proxigrams, Al and Ti partition to the γ' precipitates, while Co and Cr partition more strongly to the γ phase. The proxigrams in Fig. 4 do show a progressive change in the γ' precipitate composition while undergoing isothermal annealing post extreme water quenching (EWQ). Thus when compared with EWQ sample, 60 minutes annealing at 760 ºC changes the Ti and Al content in γ' precipitates from 8.46% to 10.56 at% and 9.33 to 10.27 at%, respectively. Conversely, the concentration of Cr and Co significantly decreases (7.57 to 2.88 at% and 9.29 to 5.96 at%, respectively). These results demonstrate that the γ' precipitates start with a far-from equilibrium composition and on subsequent isothermal annealing gets enriched in Ti and Al and depleted in Cr and Co to reach a near-equilibrium composition [Table 1].

The γ matrix follows an opposite trend where the concentration of Al and Ti slightly decreases and that of Cr and Co significantly increases on annealing for 60 minutes [Table 2]. As a result of its low diffusivity, in all cases Mo shows the least partitioning among the major alloying elements in Rene 88 DT.

Furthermore, the proxigrams in Fig. 4(a) and (b) do show a local increase in the Cr and Co contents and depletion in Al and Ti contents on the γ side of the order-disorder interface. However at distances further away from the interface, the Cr and Co contents reduce while the Al and Ti contents increase. This effect is due to the fact that only local equilibrium has been established near the γ/γ' interface in the early stages of annealing (1min and 5 min). However for these short annealing times, non-equilibrium far-field γ compositions are observed. This phenomenon is not observed in samples annealed for longer time periods (30min and 60min) due the establishment of long-range equilibration in the γ matrix, evident from Figs. 4(c) and (d), respectively.

Comparing all the proxigrams shown in Fig. 4, in the EWQ+60 case (Fig. 4(d)), the compositions of γ and γ' phases are nearest to equilibrium. This can be concluded by comparing the phase compositions in this sample with those reported previously for a 760°C/50 hrs long-term annealed Rene 88 sample [19]. Furthermore, based on both the 3D APT reconstructions shown in Fig. 4 as well as dark-field images shown in Fig. 2, the γ' precipitates exhibit a near-spherical morphology indicating the dominance of surface energy at these size scales.

The tendency for phase separation within the EWQ and annealed samples has been investigated via more detailed statistical analysis of the APT data collected from these samples. Thus, for each APT reconstruction dataset, several 100 atom bins are chosen and the composition of these bins for one specific constituent (Cr was chosen in this case) is plotted with respect to the number of bins for that particular composition. In a random solid solution, such a frequency distribution plot would exactly match with the binomial distribution for a particular dataset. This technique is more commonly known as the Langer, Bar-on and Miller (LBM) method [22,23]. The presence of a phase separation or compositional clustering within the dataset leads to a deviation from the perfect binomial distribution and is usually manifested as a peak broadening eventually leading to one or more splits developing in the peak.

Using the LBM method, the frequency distribution plot for a dataset corresponding to a phase separated system, exhibiting a split peak, can be fitted to two Gaussian distribution functions of equal width, σ, centered at concentrations, μ_1 and μ_2. The composition amplitude, ΔC, is given by $\mu_2 - \mu_1$. Note, that this method gives only an approximate estimate of the phase compositions. In this study, c_0 is estimated as the average composition (bulk composition) of Cr in the alloy, μ_1 and μ_2 are the compositions of the γ' and γ phases, and $f_{\gamma'}$ and f_γ are the estimated volume fractions of these phases, respectively.

Fig. 5 shows the compilation of different frequency distribution plots corresponding to the extreme water quenched (EWQ), 1 min annealed (EWQ+1), 5 min annealed (EWQ+5), 30 mins annealed (EWQ+30) and 60 mins annealed (EWQ+60) samples. The corresponding estimated parameters (namely μ_1, μ_2, σ, $f_{\gamma'}$ and f_γ) obtained from the LBM plots in Fig. 5 are summarized in Table 3. The EWQ sample does not exhibit any indication of phase separation; however, the frequency distribution plot for the EWQ sample does not fit a perfect binomial plot (not shown) either. Upon annealing, the frequency distribution initially decreases in amplitude with a broadened peak as shown in the EWQ+1 sample. After 5 min of annealing at 760°C, the frequency distribution plot exhibits the onset of peak separation, likely as a result of composition partitioning due to γ' formation. Thus, the fitted peaks of the two Gaussians correspond to the Cr concentration present in the γ and γ' phases. Similarly, the plots corresponding to EWQ+30 and EWQ+60 also clearly show two different peaks corresponding to the γ and γ' phases, thus deviating significantly from the binomial distribution corresponding to a random solid solution (not shown). In each of the EWQ+5, EWQ+30 and EWQ+60 conditions, the area under each of the curve nominally corresponds to the volume fraction of each phase. Comparing these three cases, the area under the curve with low Cr concentration (corresponding to γ' precipitates) increases with annealing time, indicating that there is an increase in volume fraction of γ' precipitates on annealing. The volume fraction of γ' can be estimated by determining the areas under the two Gaussian peaks (one for γ' and one for γ), fitted to the experimental data. The computed γ' volume fractions corresponding to the different isothermal annealing times have been listed in Table 3. The γ' volume fraction changes from 10% in the as-quenched (EWQ) condition to a maximum value of 30% in the 60 mins annealed (EWQ+60) condition. Based on solution thermodynamic models using the Pandat™ software, the equilibrium volume fraction of γ' at 760 ºC for the Rene 88 alloy has been predicted to be 43.4%. Thus, the experimentally determined maximum γ' volume fraction after 60 mins annealing at 760°C of 30% appears to be lower than the thermodynamic prediction. Possible reasons for this include; the alloy has not reached equilibrium after 760°C/60mins annealing, the Cr-depleted regions that are being attributed to the γ' phase in the APT dataset might not include all the $L1_2$ ordered regions in the sample, inaccuracies associated with the solution thermodynamic models used for this complex multi-component system.

The frequency distribution plots also clearly reveal that with increased annealing time the Cr content in the γ' precipitates progressively decreases, thus confirming that the precipitate composition goes from non-equilibrium towards equilibrium. Thus, the μ_1 values in Table 3, which are an indication of the Cr concentration in the γ' precipitates, changes from 8.8 at% in the EWQ condition to 3.7 at% in the EWQ+60 condition. Comparing these values with the previously reported Cr content ~ 1.7 at% in large near-equilibrium γ’ precipitates in a slow cooled and 760°C/50 hrs aged condition (SC50) sample [19], it is clear that even after 60 min annealing at 760°C this alloy has still not reached equilibrium. Furthermore, comparing the compositions of the γ matrix shown in Table 2, the EWQ+60 sample contains lower levels of Cr, Co, and Mo and a higher level of Ti as compared with the SC50 sample. This indicates that the γ matrix has not achieved its equilibrium composition even after 760°C/60 mins annealing and consequently the γ’ precipitates are still in their growth stage. These results substantiate the observation of a non-equilibrium volume fraction of γ’ for the EWQ+60 sample.

Summary

The present study focuses on temporal evolution of ordered γ’ precipitates, forming via a non-classical precipitation mechanism in a rapidly quenched commercial Ni-base superalloy, Rene 88 DT. The early stages of non-classical γ’ precipitation and the subsequent evolution during isothermal annealing has been investigated by coupling TEM and APT techniques. The results can be summarized as follows:

- $L1_2$ ordering within the γ’ precipitates can be observed in the as-quenched (EWQ) sample. The APT results reveal an interconnected network of Cr-rich and Cr-depleted pockets, based on isoconcentration surfaces and 2D compositional maps. The regions with the lowest Cr content, corresponding to the γ’ precipitates, were delineated by a 14 at% Cr isoconcentration surface. The compositional gradient across the γ/γ’ interface was diffuse and γ’ precipitate composition was found out to be far-from-equilibrium. These results indicate a non-classical mechanism of γ’ precipitation, mediated by composition modulations, presumably via spinodal decomposition throughout the γ matrix, followed by ordering within the Cr-depleted pockets [8,10,24].
- The morphological evolution of the ordered γ’ pockets in the as-quenched condition has been investigated as a function of isothermal annealing and results indicate that discrete precipitates appear only after annealing for at least 1 min at 760°C. Moreover, the γ’ precipitates exhibit nearly spherical morphologies with a unimodal size distribution for all annealing times. Equivalent diameters for γ’ precipitates increase with increasing annealing time.
- The compositional profiles (proxigrams) across the γ/γ’ interfaces clearly show that the γ’ phase composition has not yet reached equilibrium in the early stages of annealing. Additionally, while local equilibrium is achieved in the γ matrix near the precipitate/matrix interface, the far-field matrix composition exhibits a departure from equilibrium, involving an excess of Al and Ti and depletion of Cr and Co. The γ/γ’ interface width also becomes sharper with increasing annealing time.
- The γ’ volume fraction is far-from equilibrium in the as-quenched (EWQ) condition and increases with annealing time and approaches equilibrium. However, even after annealing for 60 mins at 760°C, the computed γ’ volume fraction from the APT results is ~ 30%, significantly lower than the value of 43% predicted by solution thermodynamic models (PANDAT™).

The results of this investigation clearly highlight the role of the decomposition pathway adopted during γ’ precipitation on the eventual microstructural evolution in a Ni-base superalloy. Thus, a non-classical mechanism of γ’ precipitation mediated by compositional modulations developing within the γ matrix, leads to a large number density of uniformly distributed precipitates which exhibit a monomodal size distribution and far-from equilibrium compositions. Subsequent isothermal annealing leads to the growth of these γ’ precipitates, while still maintaining a monomodal size distribution, and their compositions approach equilibrium. This is in contrast to previous reports of γ’ precipitation during continuous cooling at relatively slower rates, via a classical nucleation and growth mechanism, wherein the precipitates typically achieve a near-equilibrium composition right from the early stages and multiple nucleation bursts can take place, resulting in a multi-modal size distribution of the precipitates [19,25-30].

Acknowledgements

This work has been supported by the U.S. Air Force Research Laboratory (AFRL ISES Contract, contract number FA8650-08-C-5226). In addition, the authors also gratefully acknowledge the Center for Advanced Research and Technology (CART) at the University of North Texas for access to the experimental facilities used in this study.

References

[1] W.A. Soffa, D.E. Laughlin, Decomposition and ordering processes involving thermodynamically first-order order → disorder transformations, Acta Metallurgica. 37 (1989) 3019-3028.

[2] T. Sato, A. Kamio, Ordered Structures in the Early Stage of Decomposition in an Al-7. 9 mol% Li Alloy, Mat.Trans.JIM. 31 (1990) 25.

[3] J.W. Cahn, J.E. Hilliard, **Free Energy of a Nonuniform System. I. Interfacial Free Energy**, J. Chem. Phys. 28 (1958) 258-267.

[4] H. Cook, Brownian motion in spinodal decomposition, Acta Metallurgica. 18 (1970) 297-306.

[5] J.W. Cahn, J.E. Hilliard, Free Energy of a Nonuniform System. III. Nucleation in a Two-Component Incompressible Fluid, J. Chem. Phys. 31 (1959) 688.

[6] C.L. Corey, B.Z. Rosenblum, G.M. Greene, The ordering transition in Ni< sub> 3</sub> Al alloys, Acta metallurgica. 21 (1973) 837-844.

[7] A. Ardell, R.B. Nicholson, On the modulated structure of aged Ni-Al alloys: with an Appendix On the elastic interaction between inclusions by JD Eshelby‡‡ Cavendish Laboratory, University of Cambridge, England. Acta metallurgica. 14 (1966) 1295-1309.

[8] D.E. Laughlin, J.W. Cahn, Spinodal decomposition in age hardening copper-titanium alloys, Acta Metallurgica. 23 (1975) 329-339.

[9] G.B. Viswanathan, R. Banerjee, A. Singh, S. Nag, J. Tiley, H.L. Fraser, Precipitation of ordered phases in metallic solid solutions: A synergistic clustering and ordering process, Scr. Mater. 65 (2011) 485-488.

[10] D. Laughlin, W. Soffa, Exsolution, ordering and structural transformations: systematics and synergistics, Physical Properties and Thermodynamic Behaviour of Minerals, Springer, 1988, pp. 213-264.

[11] W. Soffa, D. Laughlin, Recent experimental studies of continuous transformations in alloys: an overview, (1982) 159-183.

[12] J. Zhao, M. Notis, Spinodal decomposition, ordering transformation, and discontinuous precipitation in a Cu–15Ni–8Sn alloy, Acta materialia. 46 (1998) 4203-4218.

[13] C. Capdevila, M.K. Miller, K.F. Russell, J. Chao, J.L. González-Carrasco, Phase separation in PM 2000™ Fe-base ODS alloy: Experimental study at the atomic level, Materials Science and Engineering: A. 490 (2008) 277-288.

[14] L. Tanner, H. Leamy, The microstructure of order-disorder transitions, Order-Disorder Transformations in Alloys, Springer, 1974, pp. 180-239.

[15] W. Gentry, M. Fine, Precipitation in Ni-11.1 at.% Al and Ni-13.8 at.% Al alloys, Acta Metallurgica. 20 (1972) 181-190.

[16] G. Schmitz, K. Hono, P. Haasen, High resolution electron microscopy of the early decomposition stage of Al□ Li alloys, Acta metallurgica et materialia. 42 (1994) 201-211.

[17] C. Pareige, F. Soisson, G. Martin, D. Blavette, Ordering and phase separation in Ni–Cr–Al: Monte Carlo simulations vs three-dimensional atom probe, Acta materialia. 47 (1999) 1889-1899.

[18] M.K. Miller, M.K. Miller, Atom Probe Tomography: Analysis at the Atomic Level, Kluwer Academic/Plenum Publishers New York, 2000.

[19] J. Hwang, S. Nag, A. Singh, R. Srinivasan, J. Tiley, H. Fraser, R. Banerjee, Evolution of the γ/γ' interface width in a commercial nickel base superalloy studied by three-dimensional atom probe tomography, Scr. Mater. 61 (2009) 92-95.

[20] P.P. Camus, D.J. Larson, Median-style filters for noise reduction in composition analyses, Appl. Surf. Sci. 76 (1994) 416-423.

[21] D. Larson, D. Foord, A. Petford-Long, H. Liew, M. Blamire, A. Cerezo, G. Smith, Field-ion specimen preparation using focused ion-beam milling, Ultramicroscopy. 79 (1999) 287-293.

[22] J.S. Langer, M. Bar-on, H.D. Miller, **New computational method in the theory of spinodal decomposition**, Phys. Rev. A. 11 (1975) 1417–1429.

[23] M. Hetherington, J. Hyde, M. Miller, G. Smith, Measurement of the amplitude of a spinodal, Surf. Sci. 246 (1991) 304-314.

[24] D.E. Laughlin, W. Soffa, Spinodal structures, ASM Handbook. 9 (1985) 652-654.

[25] P. Sarosi, B. Wang, J. Simmons, Y. Wang, M. Mills, Formation of multimodal size distributions of γ′ in a nickel-base superalloy during interrupted continuous cooling, Scr. Mater. 57 (2007) 767-770.

[26] J. Tiley, G.B. Viswanathan, R. Srinivasan, R. Banerjee, D.M. Dimiduk, H.L. Fraser, Coarsening kinetics of γ′ precipitates in the commercial nickel base Superalloy René 88 DT, Acta Materialia. 57 (2009) 2538-2549.

[27] J. Tiley, G. Viswanathan, J. Hwang, A. Shiveley, R. Banerjee, Evaluation of gamma prime volume fractions and lattice misfits in a nickel base superalloy using the external standard X-ray diffraction method, Materials Science and Engineering: A. 528 (2010) 32-36.

[28] Y. Wen, J. Simmons, C. Shen, C. Woodward, Y. Wang, Phase-field modeling of bimodal particle size distributions during continuous cooling, Acta materialia. 51 (2003) 1123-1132.

[29] A. Singh, S. Nag, J. Hwang, G. Viswanathan, J. Tiley, R. Srinivasan, H. Fraser, R. Banerjee, Influence of cooling rate on the development of multiple generations of γ′ precipitates in a commercial nickel base superalloy, Mater Charact. 62 (2011) 878-886.

[30] T. Rojhirunsakool, S. Meher, J. Hwang, S. Nag, J. Tiley, R. Banerjee, Influence of composition on monomodal versus multimodal γ′ precipitation in Ni–Al–Cr alloys, J. Mater. Sci. 48 (2013) 825-831.

Table 1. Compositions of the γ' precipitates as a function of annealing time obtained from the proxigrams for EWQ, EWQ+1, EWQ+5, EWQ+30,EWQ+60, and SC50 Rene 88 DT samples.

Sample	EWQ		EWQ + 1		EWQ + 5		EWQ + 30		EWQ + 60		SC 50 hrs	
Ion Type	Comp at%	Error %	Comp at%	Error %	Comp at%	Error %	Comp at%	Error %	Comp at%	Error %	Comp at%	Error %
Al	8.46	0.04	8.41	0.03	9.51	0.03	10.32	0.04	10.56	0.01	12.32	0.95
Ni	61.63	0.10	61.39	0.10	65.30	0.09	68.32	0.12	65.85	0.03	62.25	2.58
Mo	2.01	0.01	2.20	0.01	2.36	0.01	0.98	0.01	2.46	0.00	2.96	0.45
Co	9.29	0.04	9.64	0.03	6.41	0.02	5.6	0.03	5.96	0.00	6.52	0.68
Cr	7.57	0.03	7.27	0.03	5.16	0.02	3.02	0.02	2.88	0.00	1.71	0.34
Ti	9.33	0.04	9.09	0.03	9.47	0.03	10.22	0.04	10.27	0.01	9.22	0.81

Table 2. Composition of the γ phase obtained from the proxigrams for EWQ, EWQ+1, EWQ+5, EWQ+30, EWQ+60, and SC50 Rene 88 DT samples.

Sample	EWQ		EWQ + 1		EWQ + 5		EWQ + 30		EWQ + 60		SC 50 hrs	
Ion Type	Comp at%	Error %	Comp at%	Error %	Comp at%	Error %	Comp at%	Error %	Comp at%	Error %	Comp at%	Error %
Al	4.05	0.01	4.03	0.01	3.07	0.01	2.36	0.01	2.79	0.00	2.71	0.53
Ni	54.34	0.03	54.44	0.03	52.17	0.05	50.19	0.06	52.52	0.02	43.43	2.50
Mo	2.72	0.01	2.76	0.01	3.16	0.01	3.23	0.01	4.04	0.00	6.52	0.83
Co	13.48	0.01	13.42	0.01	14.67	0.02	16.06	0.03	15.10	0.01	19.26	1.52
Cr	19.28	0.02	19.28	0.01	22.10	0.03	24.60	0.04	21.31	0.01	23.27	1.7
Ti	4.27	0.00	4.03	0.00	2.94	0.01	1.80	0.01	2.21	0.00	0.8	0.28

Table 3. Estimated parameters of the LBM fit to the frequency distributions as a function of Cr concentration.

Sample	**c_0 (%)**	**μ_1 (%)**	**μ_2 (%)**	**σ (%)**	**f_{γ} (%)**	**$f_{\gamma'}$ (%)**	**Interface width with respect to Cr**
EWQ	17.84	8.8	18.8	3	90	10	2.4
EWQ+1	17.50	8.5	19.5	3	82	18	2.1
EWQ+5	17.59	7.6	22.6	4	80	20	2.1
EWQ+30	17.01	5	23	3	74	26	2.1
EWQ+60	17.67	3.7	24.7	3	70	30	1.6

Figure captions

Fig. 1. a) SAD pattern of the rapidly cooled Rene 88 DT sample (EWQ) showing the superlattice spots, as well as the fundamental reflections that correspond to the γ’ and γ phases. b) APT reconstruction delineating the Cr-rich and Cr-depleted regions and the 2D concentration map of Cr showing the interconnected Cr networks. c) Proxigram corresponding to the 14 at% Cr isosurface for the major alloying elements.

Fig. 2. Dark field images and SAD patterns of the rapidly cooled Rene 88 DT sample followed by annealed at 760 °C for a) 1 min, (EWQ+1), b) 5min, (EWQ+5), c) 30 min, (EWQ+30), and d) 60 min, (EWQ+60).

Fig. 3. Frequency size distribution of γ’ precipitates using dark field images for rapidly cooled samples followed by annealed at 760 °C for a) 1 min b) 5mins c) 30 mins and d) 60mins.

Fig. 4. APT reconstructions of the 14 at% Cr isosurface with Ni atoms (shown in green) and proxigrams corresponding to the 14 at% Cr isosurface of Cr, Co, Mo, Ti, and Al in the rapidly cooled samples, followed by annealing at 760 °C for a) 1 min, (EWQ+1), b) 5min, (EWQ+5), c) 30 min, (EWQ+30), and d) 60 min, (EWQ+60).

Fig. 5. Normalized LBM plot showing the phase separation of Cr as a function of annealing time.

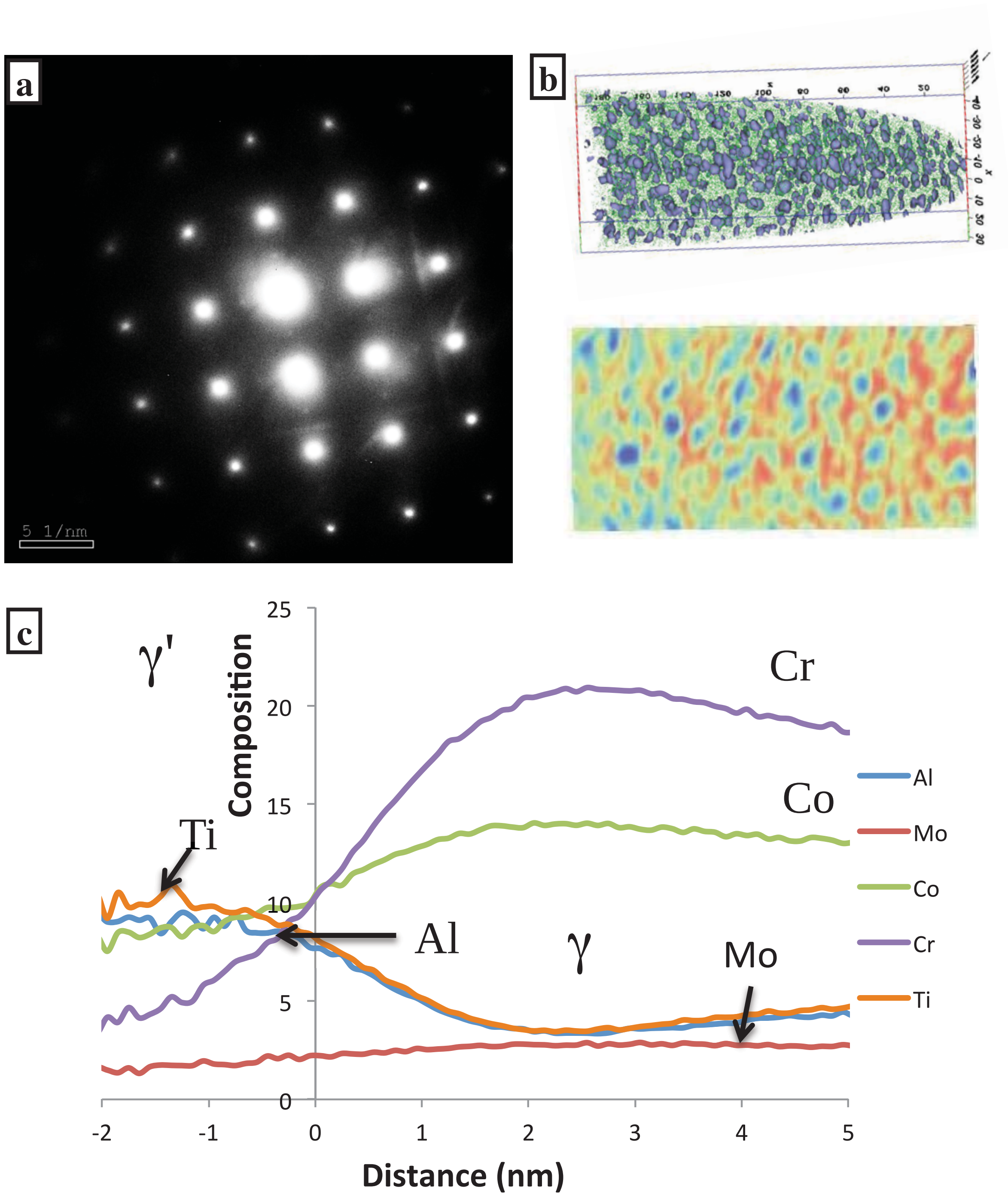

Fig. 1. a) SAD pattern of Rene 88 DT rapidly cooled sample (EWQ) shows the superlattice spots as well as the fundamental reflections correspond to the g' and g' phase. b) APT reconstruction delineating the Cr-rich and Cr-depleted regions and 2D Cr concentration map show interconnected of Cr network. c) Proxigram corresponding to 14%Cr isosurface for major alloying elements

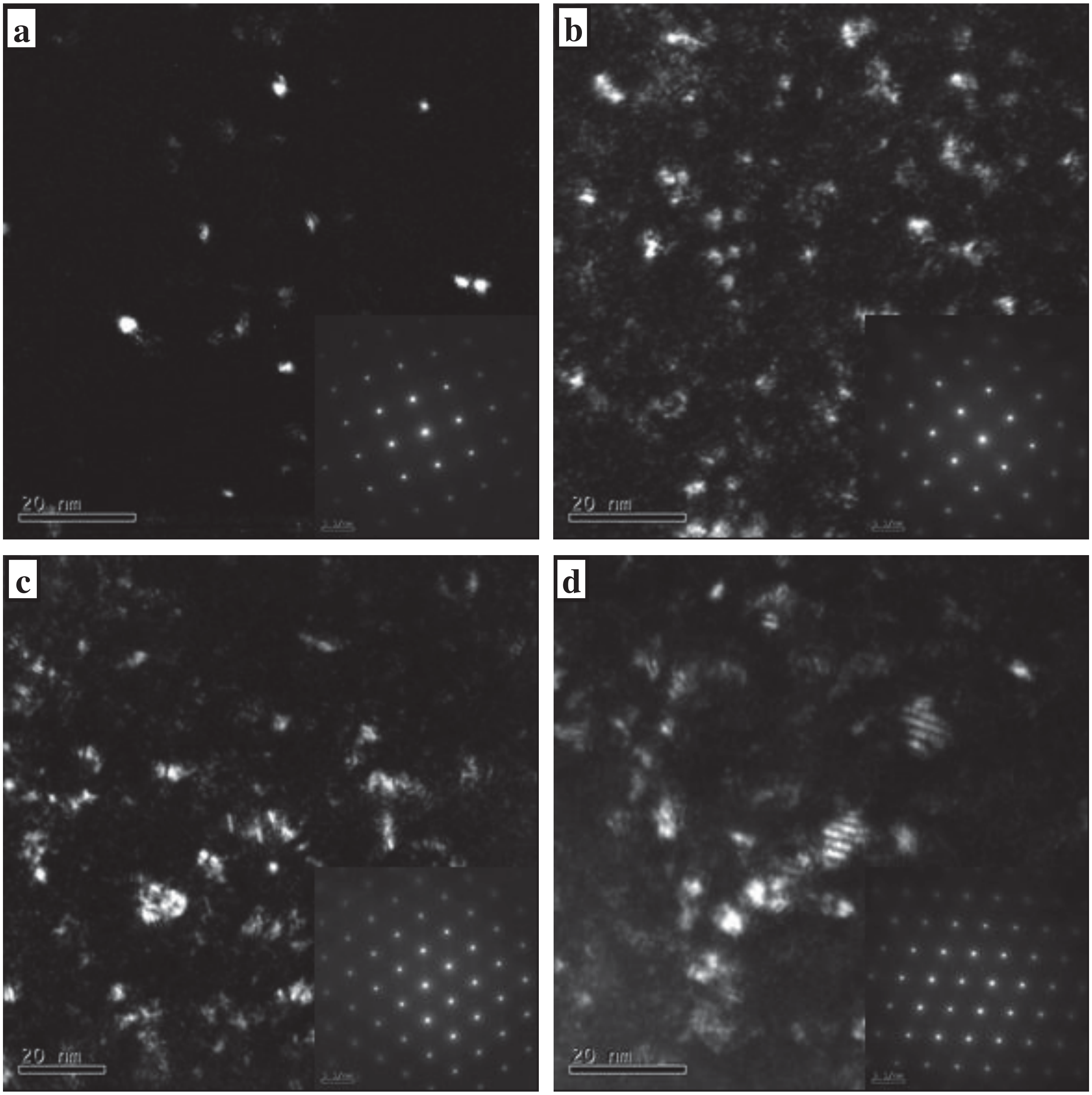

Fig. 2. Dark field images and SAD patterns of Rene 88 DT rapidly cooled sample followed by annealed at 760 °C for a) 1 min b) 5mins c) 30 mins and d) 60mins.

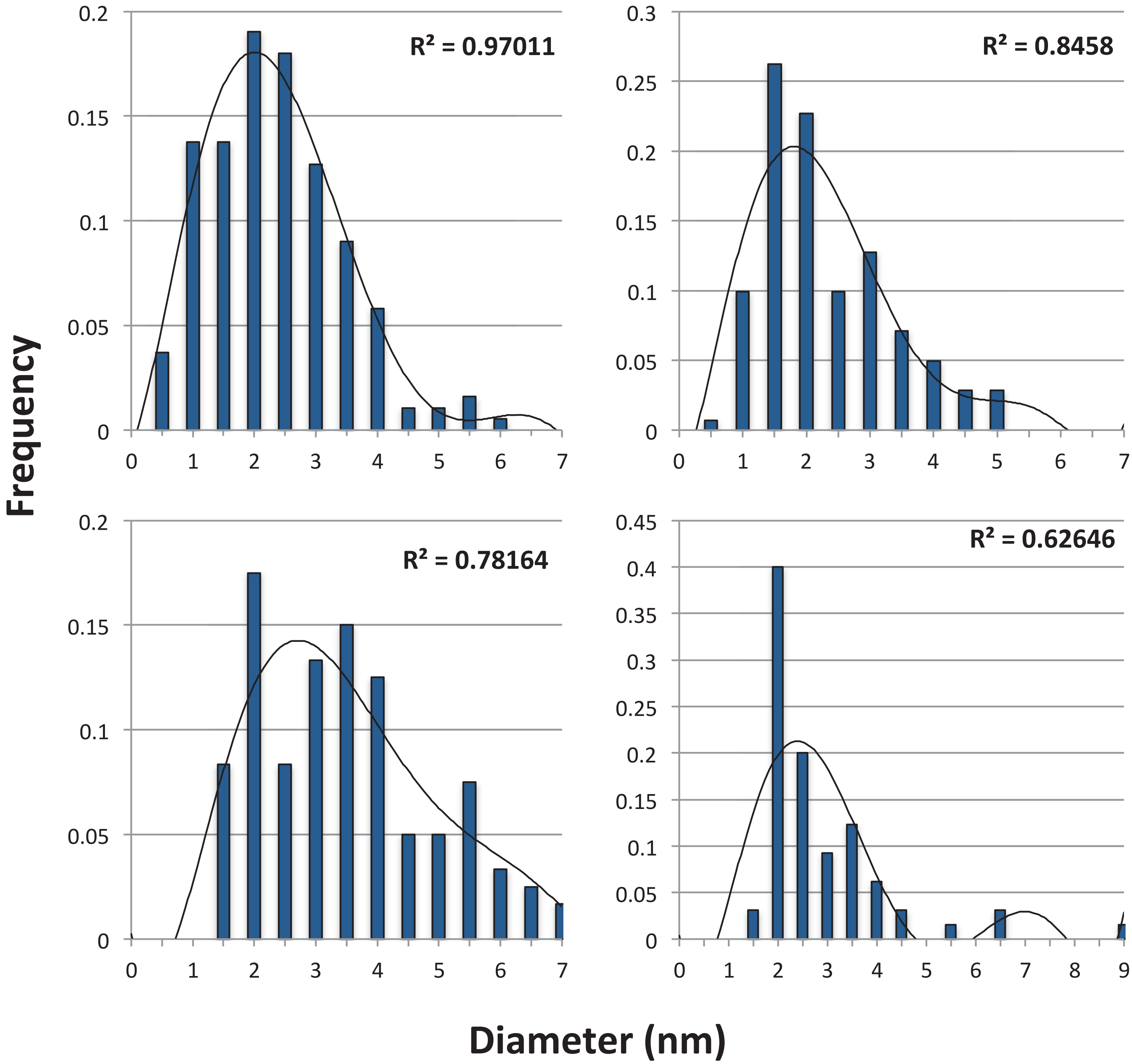

Fig. 3. Frequency size distribution of g' precipitates using dark field images for rapidly cooled samples followed by annealed at 760 °C for a) 1 min b) 5mins c) 30 mins and d) 60mins.

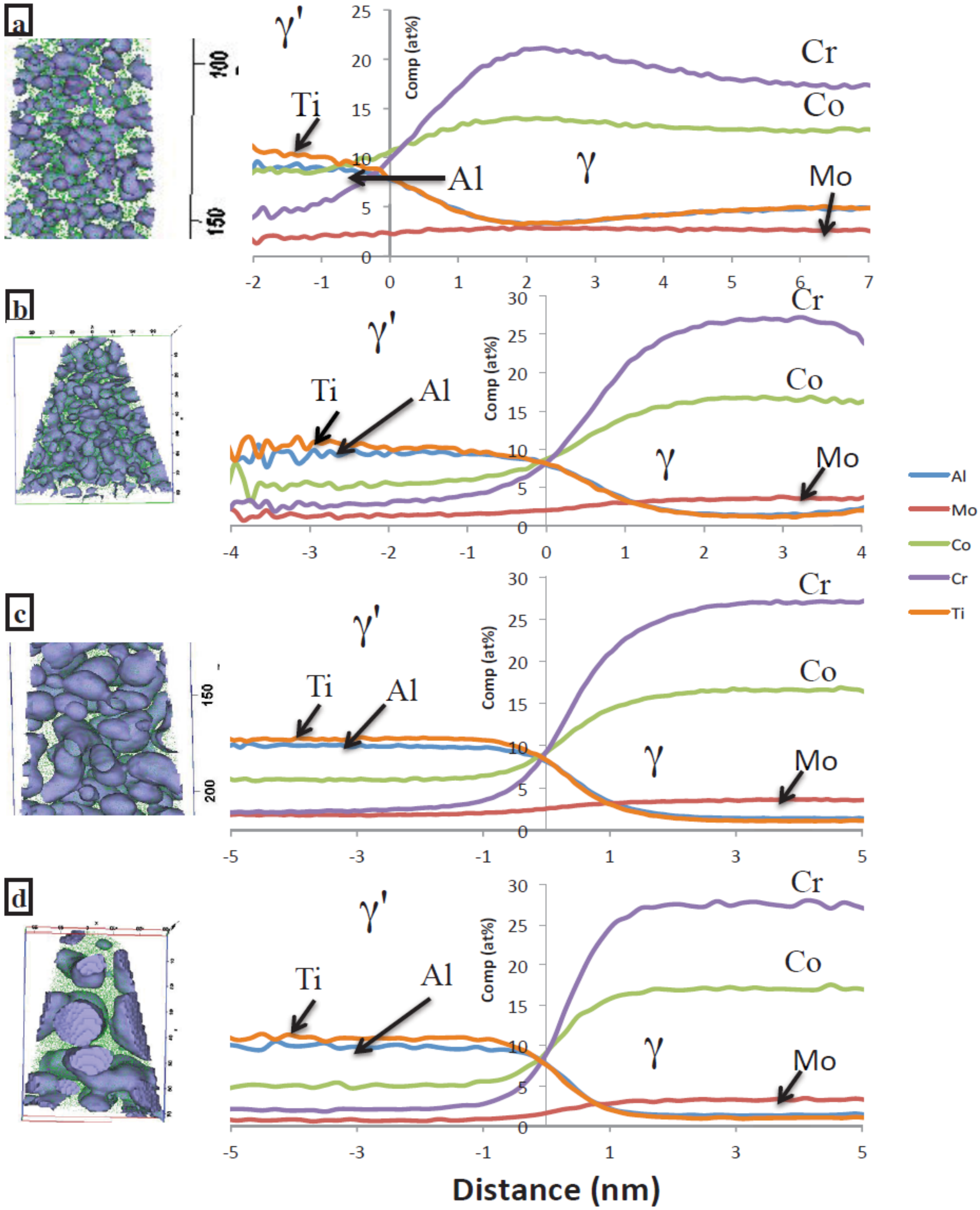

Fig. 4. APT reconstructions of 14% Cr isosurface with Ni atoms (green) and proxigrams corresponding to 14 at% Cr isosurface of Cr, Co, Mo, Ti, and Al in rapidly cooled samples followed by annealed at 760 °C for a) 1 min b) 5mins c) 30 mins and d) 60mins.

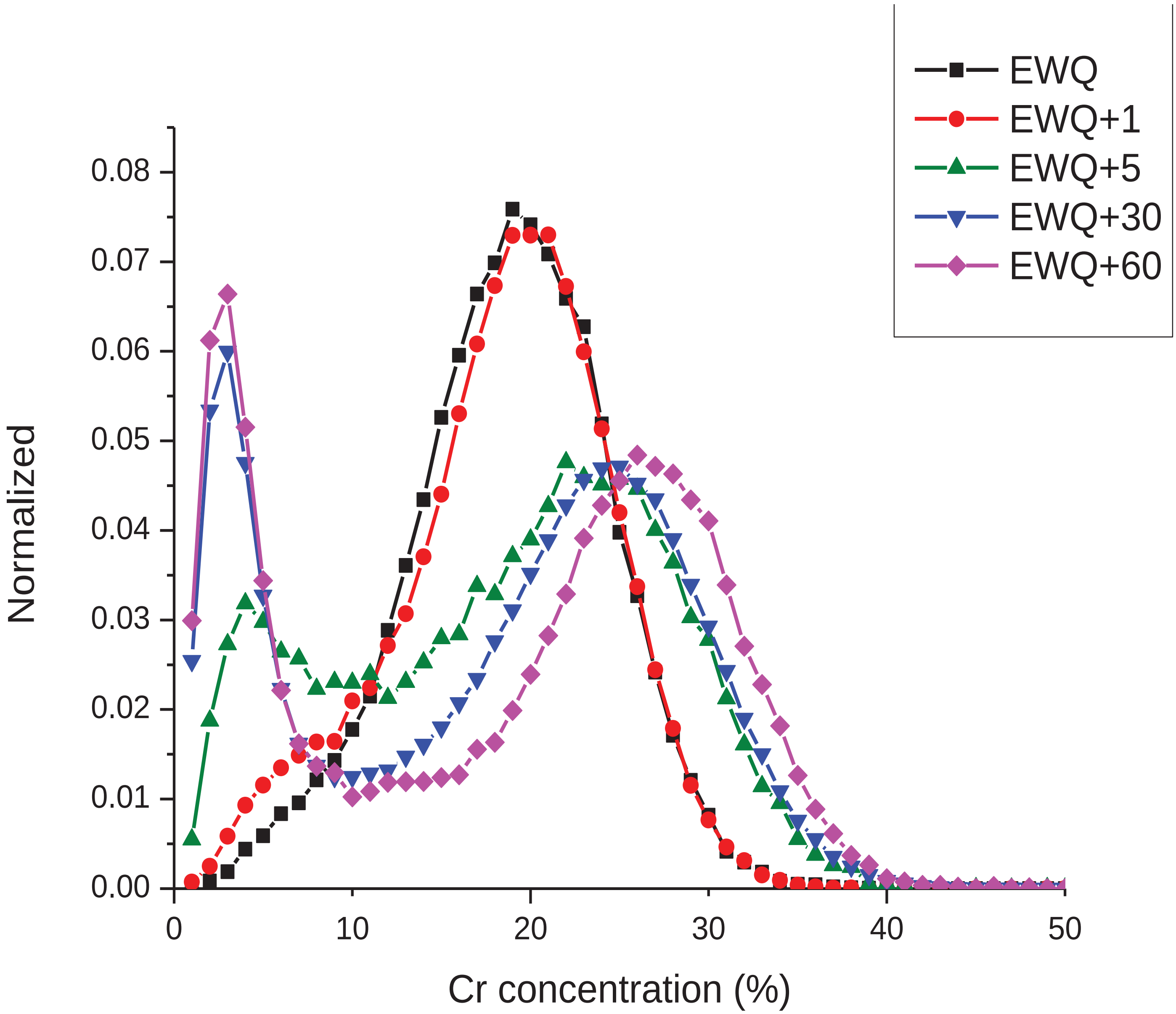

Fig. 5. Normalized LBM plot showing the phase separation of Cr as a function of annealing time